INTERNATIONAL JOURNAL OF MARITIME TECHNOLOGY
IJMT Vol.2/ Summer 2014 (1-13)
Available online at: http://ijmt.ir/browse.php?a_code=A-10-39-4&sid=1&slc_lang=en

Simulation of Wave Propagation over Coastal Structures Using WCSPH Method

Amin Mahmoudi[1], Habib Hakimzadeh[2*], Mohammad Javad Ketabdari

[1]*Ph.D. Student, Faculty of Civil Engineering, Sahand University of Technology, Tabriz; a.mahmoodi@sut.ac.ir*
[2]*Associate Professor, Faculty of Civil Engineering, Sahand University of Technology, Tabriz; Hakimzadeh@sut.ac.ir*
[3]*Associate Professor, Faculty of Marine Technology, Amirkabir University of Technology, Tehran, Ketabdar@aut.ac.ir*

ARTICLE INFO

Article History:
Received: 4 Aug. 2013
Accepted: 21 Jan. 2014
Available online: 22 Sep. 2014

Keywords:
Sea wall
Submerged breakwater
Wave propagation
WCSPH Method
LES Method

ABSTRACT

In this paper a space-averaged Navier–Stokes approach was deployed to simulate the wave propagation over coastal structures. The developed model is based on the smoothed particle hydrodynamic (SPH) method which is a pure Lagrangian approach and can handle large deformations of the free surface with high accuracy. In this study, the large eddy simulation (LES) turbulent model was coupled with the weakly compressible version of the smoothed particle hydrodynamics (WCSPH) method to simulate the wave propagation over coastal structures. The WCSPH model was employed to simulate the periodic wave propagation over impermeable trapezoidal sea wall and submerged breakwater. The numerical model results were validated against the experimental and numerical data found in the literatures and some relatively good agreements were observed. Afterwards, solitary wave propagation over impermeable trapezoidal sea wall on a sloped bed was carried out and the results of numerical simulations were compared both qualitatively and quantitatively with experimental data of Hsiao and Lin (2010). The results of this study show that WCSPH method provides a useful tool to investigate the wave propagation over coastal structures.

1. Introduction

Design of the breakwaters that allow overtopping has many benefits and is being given great attention in practice. The happening of wave overtopping if not considered in design procedure leads to a violent natural phenomenon which can cause failure of the structures and damage to the properties and life. The overtopping waves may break, often subjected to the large deformation of free surfaces. The real situations are highly complex, involving the complicated physical settings, the turbulence and eddy vortices, and the strong interactions between the wave and structure [2]. For the last few decades, submerged breakwaters have been extensively used in coastal zones for shoreline protection and to prevent beach erosion. These coastal structures mainly cause waves to break partially and thereby absorb some of its energy. There will remain some of the energy which is partly reflected and partly transmitted to shoreward [3]. Using of such constructions involves multiple benefits like reduction of coastal erosion, cost of coastal constructions, overtopping and force.

So far, some theoretical or numerical models have been developed for both the permeable or impermeable coastal structures. Stansby (2003), presented a semi-implicit finite volume method for solving the nonlinear shallow water equations with the incorporation of Boussinesq terms in a novel manner. He simulated run up, run down and overtopping on impermeable surface of variable slope [4].Li et al.(2004) carried out a detailed investigation into the wave overtopping of a sea wall by solving the N–S equations coupled with VOF surface tracking scheme and LES modeling technique [5]. Shen et al. (2004) developed a RANS model to predict the propagation of conical waves over a submerged bar. In this model, $k-\varepsilon$ turbulence model and VOF surface tracking scheme were coupled with their solver [6]. Kato et al. (2005) examined the behaviors of waves impinging on a sea wall, but did not account for the corresponding free surface measurements [7].

The performance of submerged breakwater was studied using the boundary-value problem by Rambabu and Mani (2005) [8]. Christou et al. (2008)

studied the behavior of nonlinear regular waves interacting with rectangular submerged breakwaters based on a Boundary Element Method (BEM) [9]. Jie et al. (2010) investigated characteristics of flow field and wave transmission near a submerged breakwater on a sloping bed by solving the N–S equations along with PILC-VOF surface tracking scheme and $k-\varepsilon$ turbulence model [10]. Wiryanto (2010) developed a linear model of wave propagation passing over a submerged porous breakwater for monochromatic and solitary waves associated with two coupled boundary-value problems [11].Also, Hsiao and Lin (2010) investigated tsunami-like solitary waves impinging and overtopping on impermeable trapezoidal seawall with a sloping beach in front, using both the experimental and numerical analyses. Their numerical modeling was based on RANS equations and the $k-\varepsilon$ turbulence model [1].

The Lagrangian grid-based methods may not be suitable for analyzing the flows with highly deformed free surfaces due to grid distribution. On the other hand, the Eulerian grid based methods need a proper interface capturing method to be able to simulate large and abrupt deformations with fragmentation [12].Particle methods which are among the mesh-free or gridless methods have been widely deployed in many engineering applications as well as the simulation of flow hydrodynamics. Such techniques represent the state of a system as a set of discrete particles, without a fixed connectivity, followed in a Lagrangian manner. Therefore, particle methods are intrinsically appropriate for the analysis of moving interfaces and free surfaces. Furthermore, fully Lagrangian treatment of particles, resolves the problem associated with grid-based calculations by computing the convection terms without the numerical diffusion. The method has also been extended and utilized to simulate the incompressible flows by considering the flow as slightly or weakly compressible with a proper equation of state. Run-up and run down of waves on beaches, wave breaking and overtopping on arbitrary structures and interaction between waves and coastal structures are among the applications, but mentioned a few. Some researches have been conducted, based on the SPH method, to display the feasibility of the approach when dealing with the wave and coastal structures. However, there is a few research studies dedicated to the SPH method to simulate propagation over submerged structures (for example see [16-21])

The main aim of the present paper is using WCSPH-LES model to investigate wave propagation over coastal structures, such as a submerged breakwaters and sea walls on slopping beach. To improve the WCSPH results, the Moving Least Squares (MLS) density filter was implemented in the current model.

2. Numerical Modeling

Monaghan (1992, 1994) and Liu (2003) described the main features of the SPH method in detail, which is based on the integral interpolants. The method is widely used by the researchers and thus the representation of the constitutive equations in SPH notation is only referred here [23, 24, 25]. The fundamental principle is to approximately obtain any function A(r) by:

$$A(\vec{r}) = \int_{\Omega} A(\vec{r}) W(\vec{r} - \vec{r}', h) dr' \tag{1}$$

in which, r is the vector position, W is the weighting function or kernel and h is the smoothing length. For the current numerical tests, the optimum value of the smoothing length is found to be $h = 1.3\Delta$, where Δ is the initial particle spacing.

The following function may be achieved in discrete notation due to this estimation, (particle approximation):

$$A(r) = \sum_b m_b \frac{A_b}{\rho_b} W_{ab} \tag{2}$$

The mass and density are denoted by and ρ_b, respectively and $W_{ab} = W(\vec{r}_a - \vec{r}_b, h)$ is the weighting function or kernel. The selection of weighting functions basically affects the performance of SPH model. They must satisfy some conditions such as positivity, compact support and normalization. The kernel definition is not unique, and it mainly depends on the knowledge of the investigators [23, 26]. For the current study, a Quintic function is used, which is generally employed and proposed by Wendland, (1995) [27]:

$$W(r,h) = \alpha_d \left(1 - \frac{R}{2}\right)^4 (2R+1) \qquad 0 \le R \le 2 \tag{3}$$

where α_d is $7\pi h^2/4$ in 2D, $21\pi h^3/16$ in 3D and $R = r/h$.

The Lagrangian form of the momentum conservation equation is:

$$\frac{D\vec{u}}{Dt} = -\frac{1}{\rho}\nabla P + g + \upsilon_0 \nabla^2 \vec{u} + \frac{1}{\rho}\nabla.\vec{\tau} \tag{4}$$

in which, ρ is the density, t is the time, $\vec{u}$ is the velocity vector, P is the pressure, g is the gravitational acceleration, υ_0 is the kinematic viscosity of laminar flow and τ is the Reynolds stress. The pressure gradient term in symmetrical form is expressed in SPH notation as:

$$-\frac{1}{\rho}\nabla P = -\sum_b m_b \left(\frac{P_a}{\rho_a^2} + \frac{P_b}{\rho_b^2} \right) \nabla_a W_{ab} \quad (5)$$

The laminar stress term simplifies to [13]:

$$\left(\upsilon_0 \nabla^2 \vec{u} \right) = \sum_b m_b \left(\frac{4\upsilon_0 \vec{r}_{ab} \nabla_a W_{ab}}{\left(\rho_a + \rho_b\right) \left| \vec{r}_{ab} \right|^2} \right) \vec{u}_{ab} \quad (6)$$

where $\vec{r}_{ab} = \vec{r}_a - \vec{r}_b$, $\vec{u}_{ab} = \vec{u}_a - \vec{u}_b$; being and the position and the velocity corresponding to particle k (a or b) and υ_0 is the kinetic viscosity of laminar flow ($\upsilon_0 = 10^{-6} m^2 / \sec$). SPS is deployed to model the effects of turbulence in Sub-Particle Scales [15]. Due to the fact that it preferably predicts the natural action better than the classical artificial viscosity given by Monaghan (1992), this model improves the accuracy of SPH [23]. The eddy viscosity assumption is often used for modeling the SPS stress tensor using Favre-averaging (for a compressible fluid):

$$\frac{\tau_{ij}}{\bar{\rho}} = 2\upsilon_t \tilde{S}_{ij} - \frac{2}{3}\tilde{S}_{kk}\delta_{ij} - \frac{2}{3} C_I \Delta^2 \delta_{ij} \left| \tilde{S}_{ij} \right|^2 \quad (7)$$

$$\tilde{S}_{ij} = -\frac{1}{2}\left(\frac{\partial \tilde{u}_i}{\partial x_j} + \frac{\partial \tilde{u}_j}{\partial x_i} \right) \quad (8)$$

in which, τ_{ij} is the sub-particle stress tensor, $\upsilon_t = \left(C_s . \Delta l\right)^2 . \left| \bar{S} \right|$ is the turbulence eddy viscosity, C_S is the Smagorinsky constant, Δl is the spacing between particles $\left| \bar{S} \right| = \left(2\bar{S}_{ij}\bar{S}_{ij} \right)^{0.5}$ and $\bar{S}_{ij}$ the element of SPS strain tensor.

While applying the SPH rules to calculate the element of SPS strain tensor in Eq. (7), the first derivative is estimated in the SPH formulation for any direction. For example, the discretization of the first derivative of velocity component in x direction in SPH formulation will be:

$$\left(\frac{\partial u}{\partial x} \right)_a = \sum_b \frac{m_b}{\rho_b} \left(u_b - u_a \right) \frac{\partial W_{ab}}{\partial x_a} \quad (9)$$

The choice of value for C_s is undergoing some kinds of debate. As pointed out by Yoshizawa [33], the values of C_s vary from 0.1 in the channel flow to 0.12–0.14 in the mixing layer, and up to 0.23 in the decaying turbulence. He also pointed out that some complex flows exhibit the combinations of different turbulence features and a single value of C_s cannot describe the flow accurately. In spite of these concerns, the present SPH simulations use a constant value of $C_s = 0.12$, following Dalrymple and Rogers [15] in their SPH-LES simulations of breaking waves on beaches in the two- and three-dimensions, green water overtopping of decks, and wave structure interaction. For the C_I coefficient, this value has been taken to be 0.00066, following Blinn et al. [34].

Therefore, the momentum conservation equation can be written in SPH notation as follows:

$$\frac{D\vec{u}_a}{Dt} = -\sum_b m_b \left(\frac{P_a}{\rho_a^2} + \frac{P_b}{\rho_b^2} + \frac{\tau_a}{\rho_a^2} + \frac{\tau_b}{\rho_b^2} \right) \nabla_a W_{ab} + \sum_b m_b \left(\frac{4\upsilon_0 \vec{r}_{ab} . \nabla_a W_{ab}}{\left(\rho_a + \rho_b\right) \left| \vec{r}_{ab} \right|^2} \right) \vec{u}_{ab} + g \quad (10)$$

In addition, particles are moved with the following equation:

$$\frac{d\vec{r}_a}{dt} = \vec{u}_a + \varepsilon \sum_b \frac{m_b}{\bar{\rho}_{ab}} \vec{u}_{ba} W_{ab} \quad (11)$$

where $\bar{\rho}_{ab} = \left(\rho_a + \rho_b\right)/2$ and the last term, including the parameter ε, is the so-called XSPH correction of Monaghan (1989) [28]. ε is a constant, whose values range between zero and unity, $\varepsilon = 0.5$ is often used [35].

The fluid in a standard SPH formulation is assumed to be compressible, allowing the use of an equation of state to determine fluid pressure, which is much faster than solving a differential equation like the Poisson's equation. However, the compressibility is adjusted to decelerate the speed of sound such that the time step in the model (based on the speed of sound) becomes reasonable. Fluid density change, in preference to use a weighted summation of mass terms, is calculated as below:

$$\frac{d\rho_a}{dt} = \sum_b m_b u_{ab} \nabla_a W_{ab} \quad (12)$$

This is due to the fact that it will result in an artificial density decrease as fluid interfaces are approached. The following equation shows the relationship between pressure and density by Tait's equation of state [24]:

$$P = B\left[\left(\frac{\rho}{\rho_0} \right)^{\gamma} - 1 \right] \quad (13)$$

in which γ is 7, B is $c_0^2 \rho_0 / \gamma$, ρ_0 is 1000 kg/m^3 the reference density, and c_0 is $c\left(\rho_0\right)$, the speed of sound at the reference density. For the value of sound speed, Monaghan showed that this value could artificially be slowed significantly for fluids without affecting the fluid motion. However, he suggests that the minimum sound speed should be about ten times greater than the maximum expected flow speeds [24].The parameter B was chosen to guarantee that the speed of sound becomes 16 times larger than the magnitudes of

velocities in the model. This can be achieved by taking $B = 256gh_0\rho_0/\gamma$, where h_0 is the depth of the water tank.

The pressure field of the particles shows large pressure oscillations, although the dynamics from SPH predictions are generally realistic. Several approaches have been proposed to overcome this problem. One of the simplest methods is to perform a filter over the density of the particles and the re-assign a density to each particle [29]. Then, the Moving Least Squares (MLS) approach was used for the current modeling approach. It was firstly developed by Dilts (1999) [30] and successfully applied by Colagrossi and Landrini (2003) [29] and Panizzo (2004) [31].

In this research, the Predictor-Corrector algorithm described by Monaghan (1989) [28] was used in numerical modeling with a time step set to $\Delta t = 5\times10^{-5}$ sec. This time step is small enough to satisfy the Courant condition and controlling the stability of force and viscous terms [23].

2.1. Boundary and Initial Conditions

In the SPH model, identification and tracking of free surfaces can always be simply conducted by particles. In the computational domain no special treatment was applied on free surface particles. In fact, the main advantage of the SPH method is that free surface is modeled naturally.

Selecting the boundary conditions is very important in hydrodynamic problems. In this research, the condition of dynamic boundary particles (DBPs) is used in the WCSPH model. For fixed boundaries, the set of these particles is composed from fixed particles placed in a staggered grid manner [36]. The motion of these particles satisfies the governing equations (10, 12) and the equation of state (13). However, they are not allowed to move in accordance with Eq. (11). Additionally, for moving boundaries, such as wave-makers, it is necessary to impose the position and velocity of boundary particles at each time step. This type of boundary conditions is easy to apply due to its computational effortlessness where the interaction between the fluid and boundary can be calculated inside the same loops as fluid particles. Then, the following simple repulsion mechanism of DBPs is used: when a fluid particle approaches the boundary, the density of the boundary particles increases in accordance with Eq. (12), resulting in an increase in pressure following Eq. (13). Thus, the force acting on the fluid particle increases due to the pressure term P/ρ^2 in the momentum equation Eq. (10). More details were discussed in [37].

The upstream open boundary is set to be the incident wave. It is modeled by a numerical wave maker composed of wall particles. The wave maker moves periodically during the computations. The profile of a solitary wave as a function of distance x and time t is defined as:

$$\eta(x,t) = H_0 \sec h^2\left[n\left(x - Ct\right)\right] \tag{14}$$

in which C is the celerity of the wave and n is given by:

$$n = \sqrt{\frac{3H_0}{4h_0^2\left(h_0 + H_0\right)}} \tag{15}$$

$$C = \sqrt{g\left(H_0 + h_0\right)} \tag{16}$$

in which, h_0 and H_0 are deep-water depth and wave height respectively.

Generation of solitary wave was performed using a piston type wave maker. The time-dependent wave board trajectory $X(t)$ for producing a solitary wave profile is determined as:

$$X(t) = \frac{2H_0}{h_0\beta}\frac{h_0\tanh\left(\beta Ct/2\right)}{h_0 + H_0\left[1-\tanh^2\left(\beta Ct/2\right.\right.} \tag{17}$$

$$\beta = 2\sqrt{\frac{3H_0}{4h_0^2\left(H_0 + h_0\right)}} \tag{18}$$

in which β is decay coefficient [32].

In this research the initial velocity of the fluid particles was considered as zero and these particles were initially placed on a Cartesian grid with dx=dz. The particles are assigned an initial density, ρ, which needed to be adjusted to give the correct hydrostatic pressure when the pressure is calculated from the equation of state. So, Initial density of a particle would be modified taking in account the water column height as follow:

$$\rho = \rho_0\left(1 + \frac{\rho_0 g\left(H - z\right)}{B}\right)^{\frac{1}{\gamma}} \tag{19}$$

in which, H is the water depth in the tank and z is the distance of particle from bottom [14].

3. Analyses, Results and Discussion

As we mentioned above, the pressure field of the particles can exhibit large pressure oscillations, which can be smoothed out by performing a filter over the density. In order to investigate this problem in WCSPH method, a benchmark dam break test is performed without density filter and with a MLS density filter. The tank is 4 m long, the initial volume of water is 1 m long and its height 2 m. Filter were only used every m = 30 time steps.

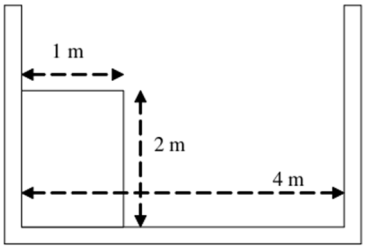

Figure 1. Initial configuration of the water column and the tank

The pressure fields obtained using MLS filters are less noisy than the ones obtained without filters (Figure 2). At t = 2 .20 s the jet in the unfiltered solution has suffered unphysical fragmentation and is different both in shape and position to the ones observed in the cases with density filters. In addition, the wave profile generated after overturning is also different. Bubble capture generated by two consecutive breakings of the reflected wave is reproduced by MLS method but not by the unfiltered method.

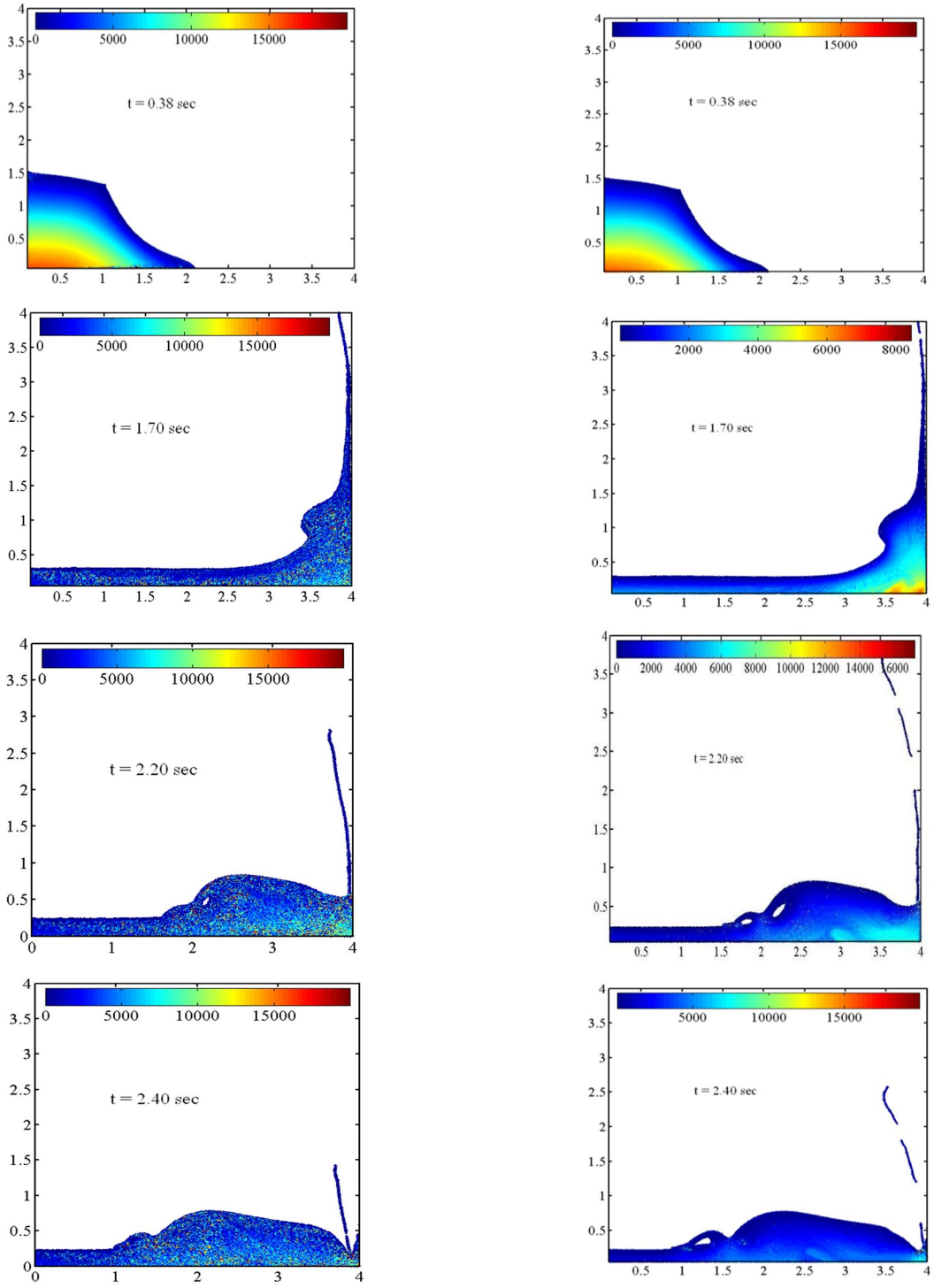

Figure 2. Dam break evolution and water overturning. Comparison among the results obtained by means of the two methods: without density filter (left side); with MLS filter (right side).The color of each particle corresponds to its instantaneous pressure (Pa)

In this paper, in order to validate the developed numerical model, three experimental data sets were used.

3.1. Wave Propagation over Impermeable Trapezoidal Sea Wall

In order to simulate the periodic wave propagation over impermeable trapezoidal sea wall on plane bed, the laboratory experimental results of Li et al. (2004) was used [5]. Figure 3 shows general layout and important parameters of their experimental work. The computational domain covering a sea wall was 6.3 m long and 1.0 m high. A regular wave with a height H =0.16 m and period T =2.0 sec was used.

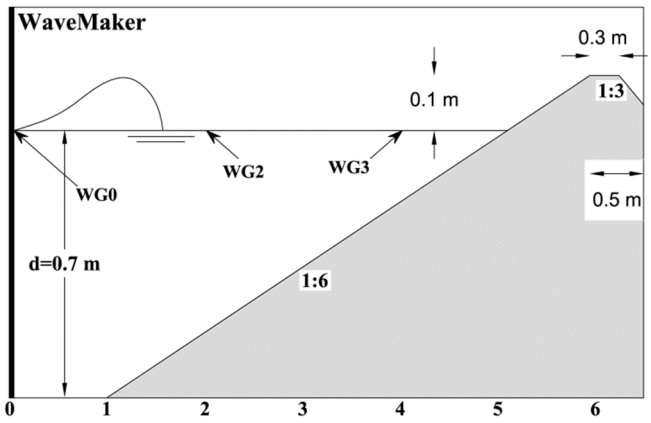

Figure3. Schematic of the numerical flume and sloping sea wall for wave breaking [5]

The WCSPH approach with LES modeling was used to investigate regular wave propagation over a smooth impermeable sea wall. Table 1 summarizes detail information about numerical modeling. For a quantitative evaluation of the SPH computations with LES modeling, the computed water surface elevations at two gauging stations are shown in Figures 4 and 5. The experimental and numerical data of Li et al. [5] are also included in the figures. Li et al. used a time-implicit cell-staggered approximately factored VOF finite volume approach for solving the unsteady incompressible N–S equations based on the non-uniform Cartesian cut-cell grids. Meanwhile, the effects of turbulence were addressed by using both static and dynamic sub-grid scale (SGS) LES turbulence models in their formulations. As shown in Figures 4 and 5, WCSPH results are better agree with experimental data than those of Li et al. [5]. This good agreement is mainly attributed to the fact that the free surface is accurately tracked by the particles without numerical diffusion in the SPH approach.

Table 1.Detail information of numerical simulation

dx and dz	0.01 m
number of particles	23636
number of boundary particles	2076
simulation time	20 sec
computational cost	2 days
Type of the used computer	CPU 2.60 GHz and RAM 2.00 MB

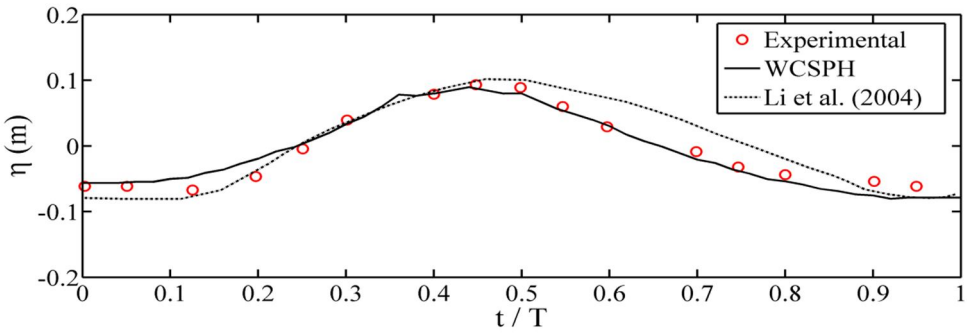

Figure 4. Comparison of computed water surface elevations by SPH with experimental and numerical data of Li et al. [5] for WG2 (x=2.02 m)

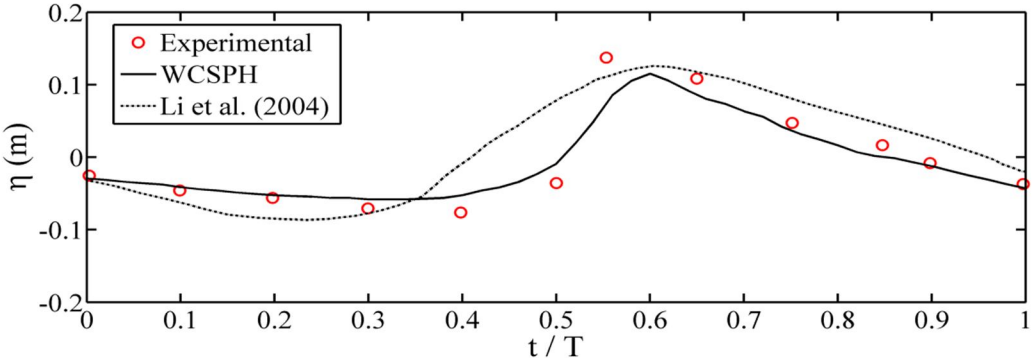

Figure 5. Comparison of computed water surface elevations by SPH with experimental and numerical data of Li et al. [5] for WG3 (x=3.81 m)

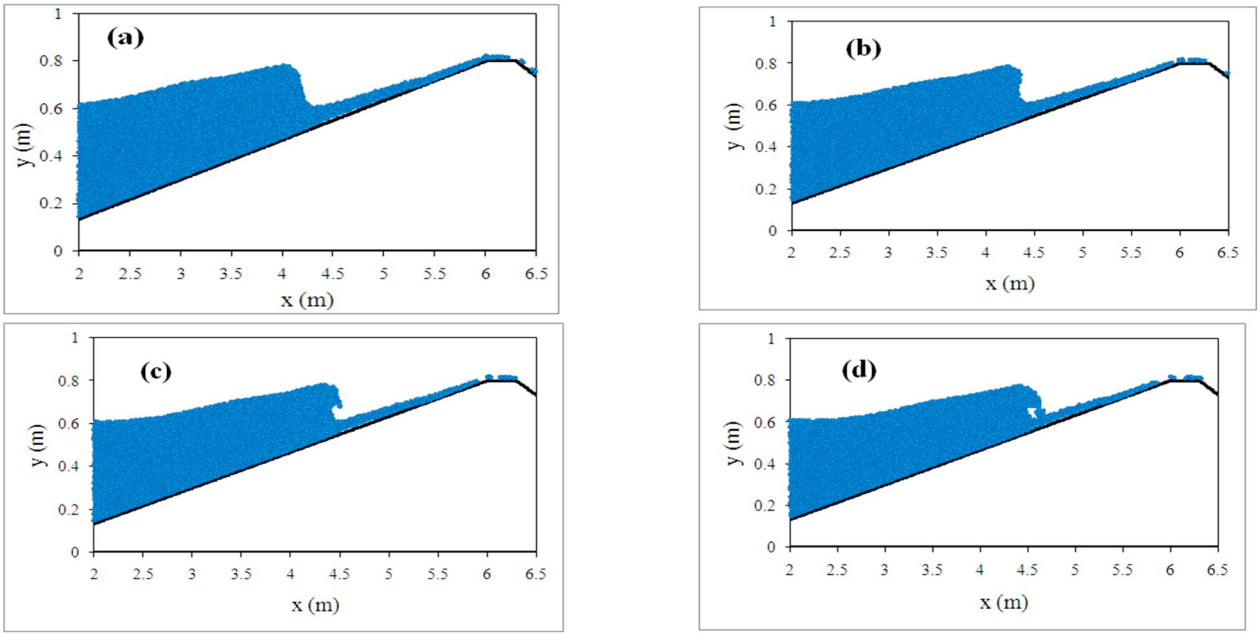

Figure 6. Particle snapshots during wave breaking: a) t=5.16 sec, b) t=5.28 sec, c) t=5.36 sec, d) t= 5.44 sec

Wave overtopping is a highly complicated process, including the wave attack, run-up, run-down, breaking and overtopping, accompanied by the large deformations of the free surface. For a general picture of the wave breaking and overtopping processes, the instantaneous particle snapshots are shown in Figure 6(a)–(d), based on the WCSPH computational results. As can be seen in Figure 6(a), some particles of the preceding wave still continue to overtop on the sea wall crest, while the majority of flows have already begun to retreat from the slope due to the gravitational acceleration. It can be seen that the general features of the wave breaking, collapsing and subsequent turbulent bore formation have been well captured by the WCSPH–LES model. The overturning of wave front at the breaking is adequately disclosed by the WCSPH computations in Figure 6(c).

The observed differences between the numerical and experimental results can be quantified by means of two statistical parameters.

$$A_r = \left(\sum_i \left(Var_i^{num} \right)^2 / \sum_j \left(Var_i^{\exp} \right)^2 \right)^{1/2} \quad (20)$$

$$P_d = \left(\sum_i \left(Var_i^{num} - Var_i^{\exp} \right)^2 / \sum_j \left(Var_i^{\exp} \right)^2 \right)^{1/2} \quad (21)$$

where"Var" is the variable that has to be considered and the superscripts refer to experimental or numerical values. The first parameter, A_r, represents the relative amplitude of both signals, in such a way that a perfect agreement between the experimental and numerical data would result in $A_r \to 1$. On the other hand, the second parameter, P_d, is the phase difference between both signals, a perfect agreement would result in $P_d \to 0$.

Table 2 summarizes the values of A_r and P_d obtained for the WCSPH (present model) and numerical data of Li et al. [5]. Although both statistical parameters show a satisfactoryagreement between the numerical and experimental solutions, however, the numerical model results show to be more accurate when using the WCSPH method.

Table 2.Statistical parameters A_r and P_d for the WCSPH (present model) and numerical data of Li et al. [5]

	SPH method		Li et al. (2004)	
	for WG2 (x=2.02 m)	for WG3 (x=3.81 m)	for WG2 (x=2.02 m)	for WG3 (x=3.81 m)
A_r	0.986	0.93	1.183	1.098
P_d	0.1698	0.215	0.3796	0.658

3.2. Wave Propagation over Submerged Breakwater

The experimental data set to simulate the periodic wave propagation over submerged breakwater, was based on the physical experiment, outlined in Ohyama et al. (1995) [22]. The experiments were performed in a wave channel of 65 m in length, 1.0 m in width, and 1.6 m in height. The still water depth was 0.5m in deep water region and 0.15 m over the top of the submerged breakwater. The detailed geometric dimensions of the submerged breakwater are also shown in Figure 7. The incident wave conditions for two representative cases as listed in Table 3, are adopted here for numerical simulation. In this table T, h and H are the wave period, water depth, and wave height respectively.

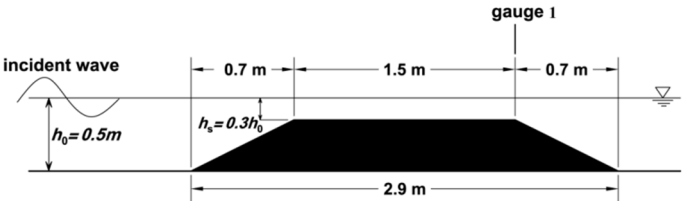

Figure 7. Sketch of submerged breakwater and location of the wave gauges [22]

Table 3. Incident wave conditions in WCSPH simulations and physical experiment [22]

Case number	$T_0\sqrt{g/h_0}$	H_0/h_0	$h_0(m)$
Case 1	5.94	0.1	0.5
Case 2	8.94	0.1	0.5

Another important phenomenon in the coastal engineering is the water wave propagation over submerged breakwaters. In this section, we investigate the periodic wave trains passing over a submerged trapezoidal breakwater using WCSPH-LES model. Table 4 summarizes detail information about numerical modeling. Figures 8 and 9 show the computed results and the corresponding experimental data at gauge 1 for the two cases listed in Table 3, where η/H_0 is the normalized wave height, and t/T_0 is the normalized time. While, the experimental data of Ohyama et al. [22] and numerical results of Shen et al. [6] are shown for comparison purpose.

Table 4.Detail information of numerical simulation

dx and dz	0.01 m
number of particles	48920
number of boundary particles	3166
simulation time	20 sec
computational cost	7 days
Type of the used computer	CPU 2.60 GHz and RAM 2.00 MB

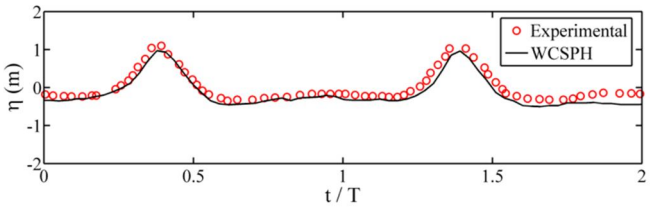

Figure 8. Comparison of estimated water surface elevations by WCSPH and experimental data of Ohyama et al.[22] for case 1.

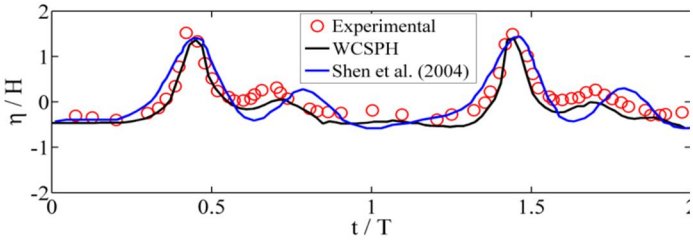

Figure 9. Comparison of estimated water surface elevations by WCSPH, experimental data of Ohyama et al. [22] and numerical data of Shen et al. [6] for case 2

It should be mentioned that Shen et al. (2004) used the VOF method with a two equations $k-\varepsilon$ turbulence model to simulate wave propagation over a submerged breakwater [6].

As shown in Figure 9, the WCSPH computations produce better results than those of Shen et al. [6], with respect to the experimental data. It can be seen that the results obtained from both of two wave cases are in good agreements with the experimental data. Of course because of the complicated flow separations and the transfer of nonlinear wave energies, there are the most difficult issues for any numerical models to predict wave transformation during the decomposition process. Although the obtained wave crest is lower than the experimental data, the general agreements between the numerical results and the experimental data are very encouraging.

Table 5 summarizes the values of A_r and P_d obtained for the WCSPH (present model) and numerical data of Shen et al. [6] for case 2. Although both statistical parameters show a satisfactory agreement between numerical and experimental solutions, however, the numerical model results show the WCSPH computations produce more reasonable numerical results than those of Shen et al. [6].

Table 5.Statistical parameters A_r and P_d for the WCSPH (present model) and numerical data of Shen et al. [6]

	WCSPH method	Shen et al. (2004)
A_r	1.013	1.138
P_d	0.319	0.497

3.3. Solitary Wave Propagation over an Impermeable Trapezoidal Sea Wall on a Sloped Bed

The third data set was based on the laboratory experiments of Hsiao and Lin (2010) to study of solitary wave propagation over an impermeable trapezoidal sea wall on a sloped bed [1]. In their experimental set up topography had two sections (Figure 10(a) and (b)). The first section was a uniform and impermeable aluminum having 1:20 slope starting 10 m from the wave paddle (i.e. x = 10 m). The other section was an impermeable trapezoidal caisson with seaward 1:4 and landward 1:1.8 slopes. The seawall model was mounted on the slope starting at a horizontal distance of 3.6 m from the beach toe (i.e. x = 13.6 m). The experimental conditions for two representative cases, are listed in Table 6.

Table 6. Incident wave height and water depth in physical model [1]

Case number	$h_0(m)$	$H_0(m)$
Case 1	0.2	0.07
Case 2	0.22	0.0638

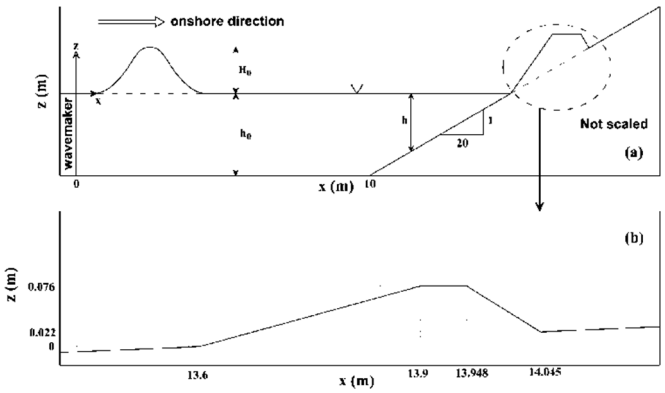

Figure 10. Sketch view of experimental setup [1]

As a tsunami-wave train propagates toward shallow water, it may form a sequence of turbulent bores or collapse upon near shore breakwaters leading to overtopping flows. Such severe breaking waves and their accompanying wave forces can cause different structure failure mechanisms. During these mechanisms, the generated turbulence and vorticity create sediment transportation and scouring near the toe of coastal breakwaters [1]. In this section, the WCSPH approach with LES modeling was employed to investigate solitary wave propagation over a smooth impermeable trapezoidal sea wall located on a sloped bed. Table 7 summarizes detail information about numerical modeling. Figure 11 compares between the analytical and the simulated wave profile for case 1. It can be seen that the numerical wave profile agrees well with the analytical one.

Table 7.Detail information of numerical simulation

dx and dz	0.005 m
number of particles	27692
number of boundary particles	3644
simulation time	10 sec
computational cost	1 days
Type of the used computer	CPU 2.60 GHz and RAM 2.00 MB

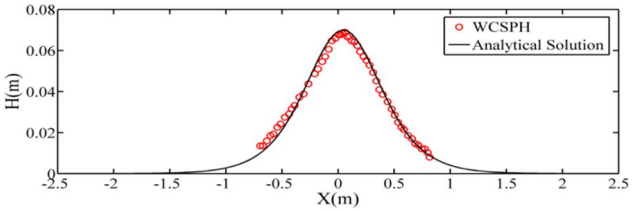

Figure 11.Comparison between the simulated and analytical wave profile for case1.

Figures 12 and 14 illustrate the solitary wave propagation over a smooth impermeable trapezoidal sea wall on a sloped bed, including wave shoaling, breaking, impingement, run-up and overtopping with the conditions corresponding to the simulation case 1 and case 2, respectively. In the left part of the figure, the still photographs are those taken during laboratory experiments [1], while particles snapshots of the WCSPH model are shown on the right hand side. Comparison of the numerical and experimental results of free surface is also shown in Figures 13 and 15 at different times for cases 1 and 2, respectively.

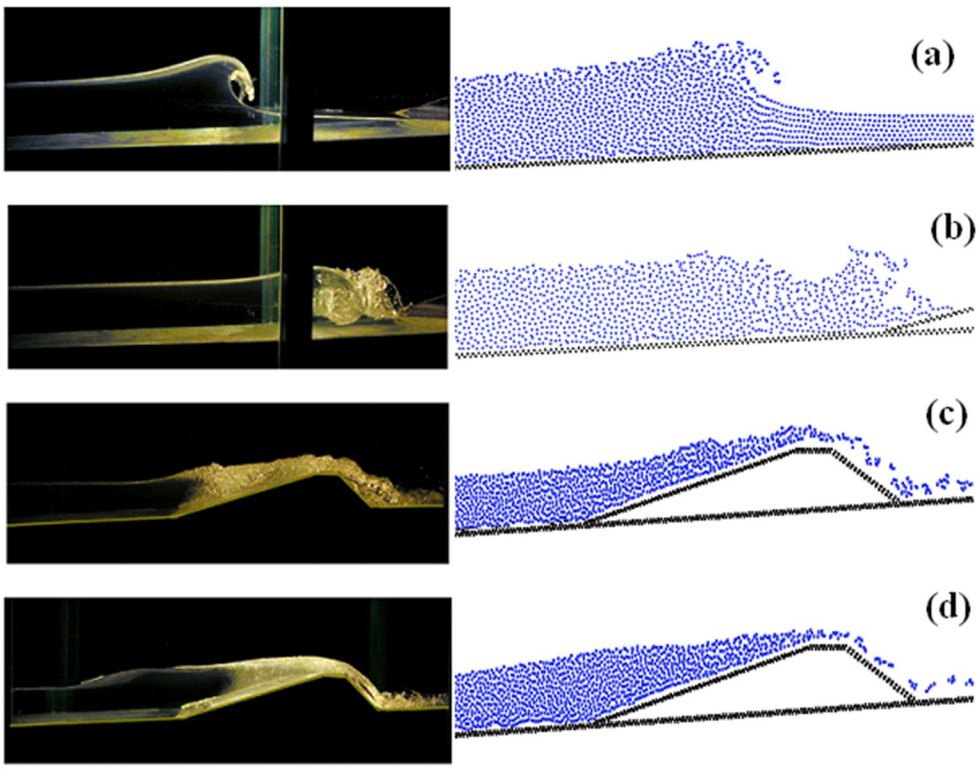

Figure12. Comparisons of free surface evolution between laboratory images (left)[1] and WCSPH particles snapshots (right) for case 1 at a) t = 2.63 s, b) t=2.89 s, c) t= 3.35 s, and d) t= 3.71 s.

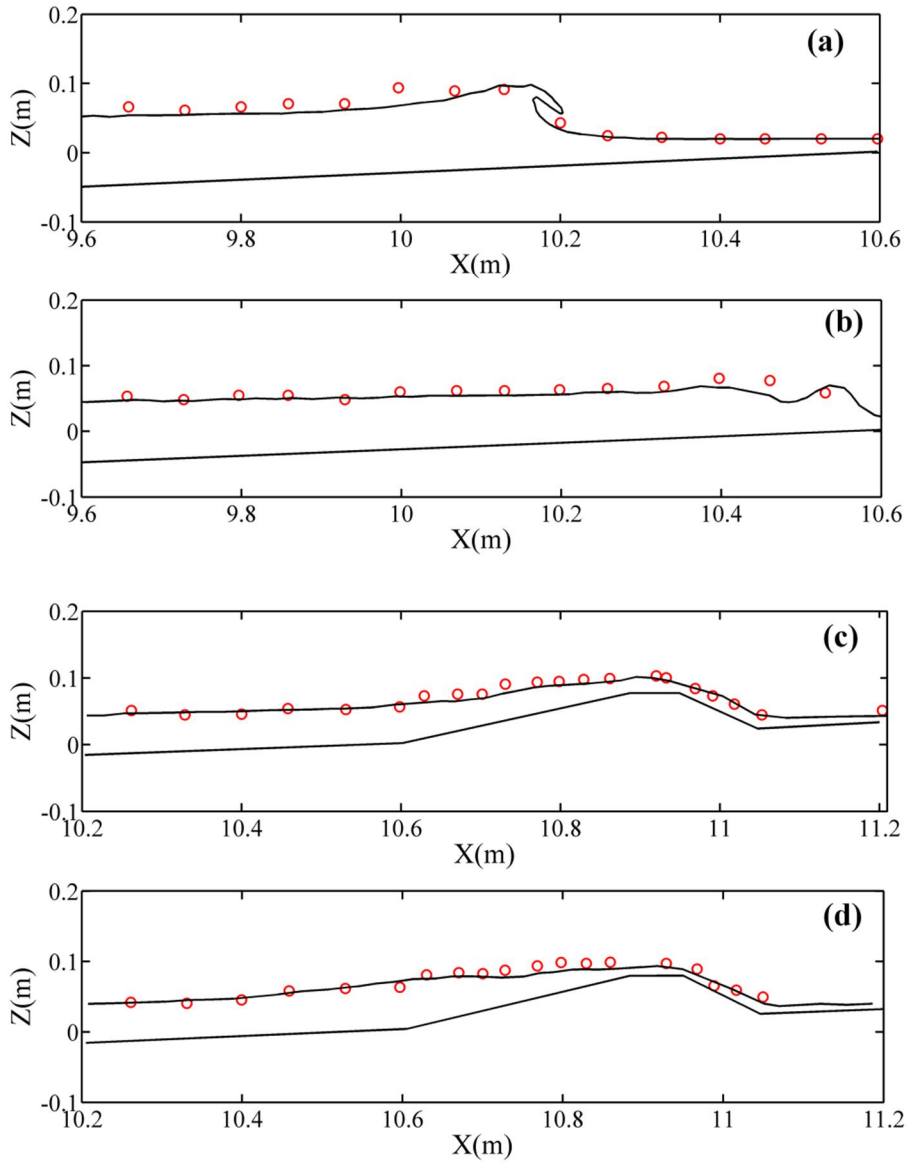

Figure 13. Comparisons of free surface evolutions between measurement data (Red circles)[1] and WCSPH model (black solid lines) for case 1 at a) t = 2.63 s, b) t=2.89 s, c) t= 3.35 s, and d) t= 3.71 s.

When a wave propagates on the slope, it is naturally influenced by shoaling as the depth of water decreases. Hence, the wave profile becomes unsymmetrical, the transmitted wave height increases, the wave crest becomes steeper and eventually it breaks. Figures 12 and 13 show that for the case 1, the breaking wave forms a turbulent bore offshore, which then impinges upon and overtops the sea wall. The incident solitary wave breaks as a plunging type, in which the wave curls over with some air.

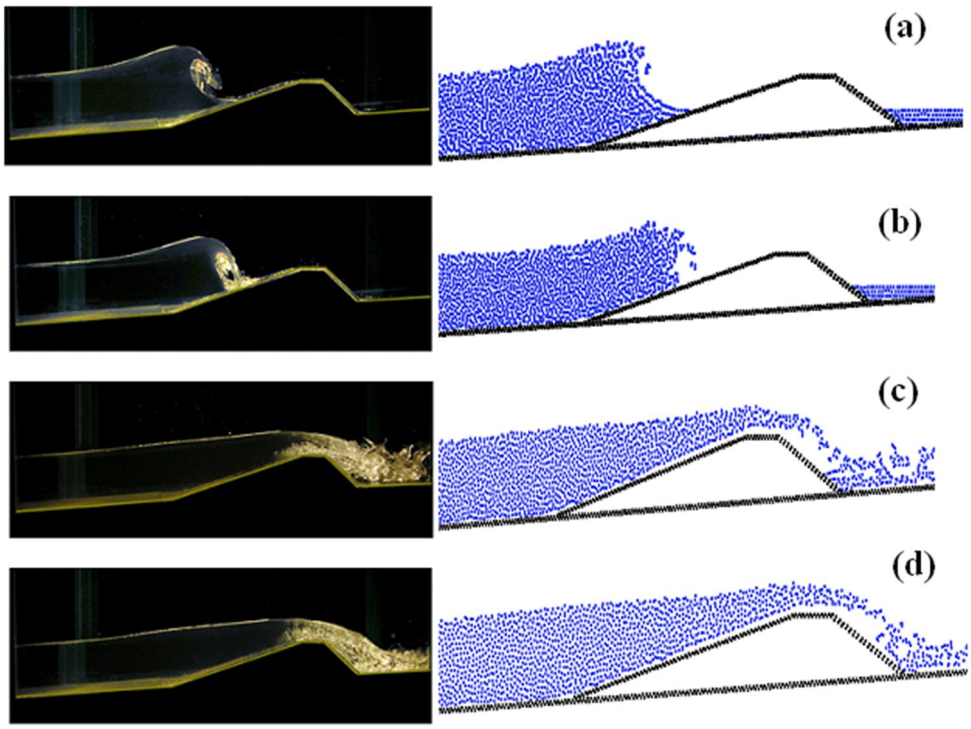

Figure 14. Comparisons of free surface evolution between laboratory images (left)[1] and WCSPH particles snapshots (right) for case 2 at a) t = 2.95 s, b) t=3.01 s, c) t= 3.22 s, and d) t= 3.34s.

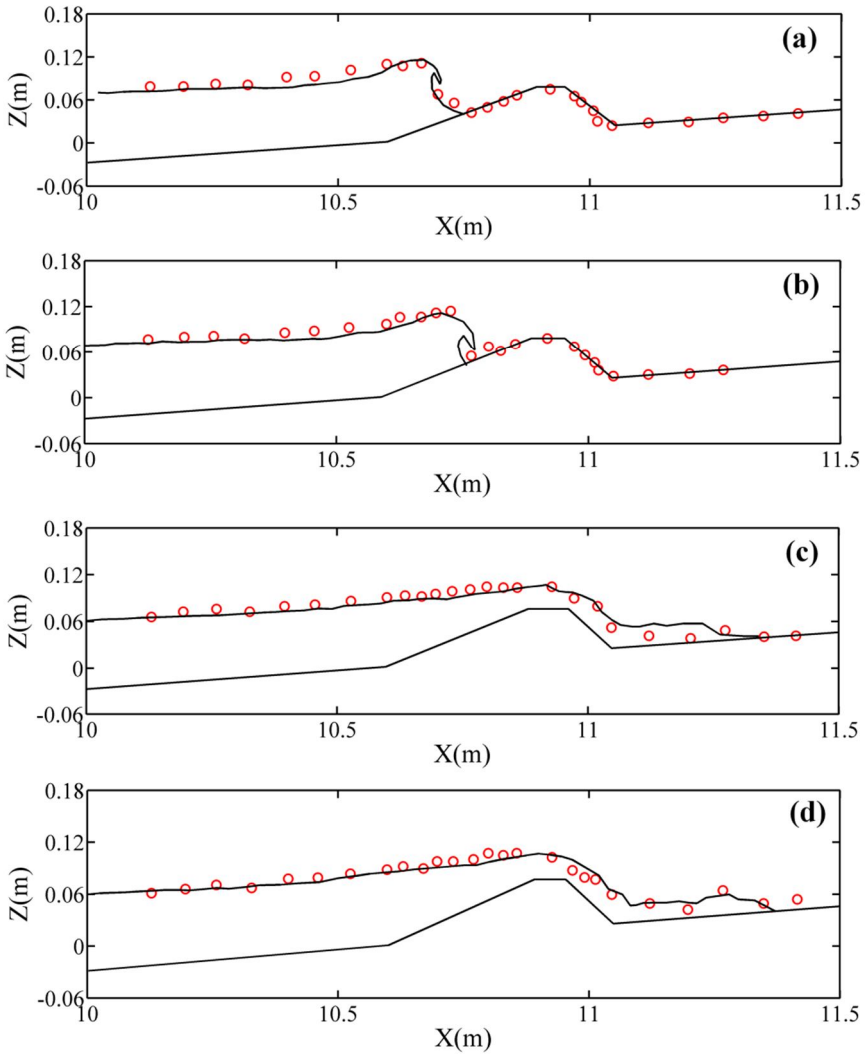

Figure 15. Comparisons of free surface evolution between measurement data (Red circles)[1] and WCSPH model (black solid lines) for case 2. Simulated free surface at a) t = 2.95 s, b) t=3.01 s, c) t= 3.22 s, and d) t= 3.34s.

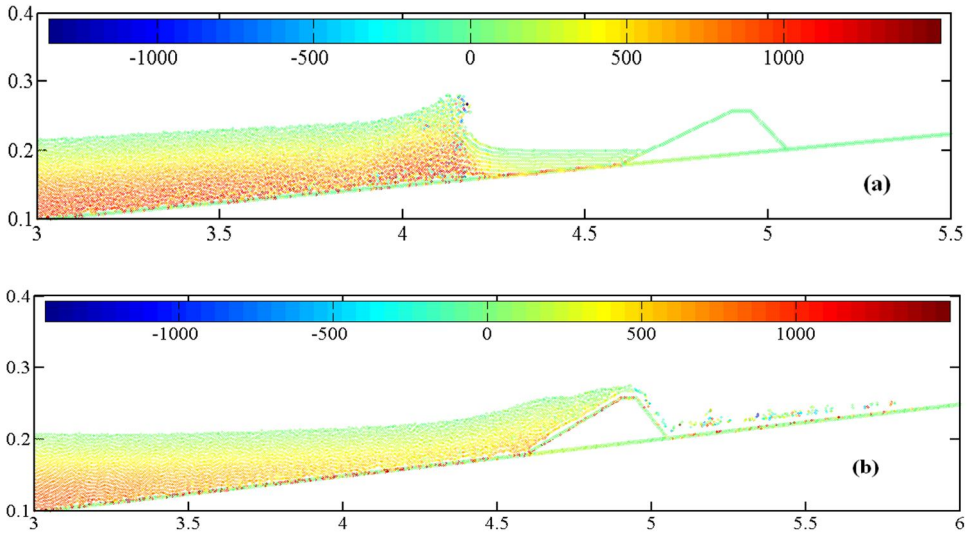

Figure 16. Pressure fields (Pa) of solitary wave propagation over an impermeable trapezoidal sea wall on a sloped bed using MLS density filter for case 1 at a) t = 2.63 s and b) t= 3.35 s

Figures 14 and 15 show that for the case 2, the wave collapses directly upon the sea wall and an overtopping flow is subsequently generated. With the same plunging breaker as that for case 1, the leading breaking front also captures considerable air and starts impacting the sea wall. The WCSPH model results show well agreement to the laboratory photographs and measurements. Simulating this type of flow with a two-phase simulation involving air should increase the quality of the presented results. Nevertheless, when the WCSPH is used to model the details of the highly nonlinear physical processes, implementation of such kind of improvements should be considered. The pressure fields obtained using MLS filters are shown in Figure 16.

4. Conclusions

In this study a WCSPH method together with a LES approach was used to simulate the wave propagation over coastal structures. The numerical simulations on solitary wave propagation over an impermeable trapezoidal sea wall on a sloped bed and the periodic wave propagation over an impermeable trapezoidal sea wall and submerged breakwater were carried out. The results showed that simulated model results are in good agreement with experimental data. Comparisons between WCSPH results with the conducted laboratory photographs tentatively illustrate the capability of the WCSPH method in the simulation of wave propagation over coastal structures. The WCSPH computations lead to better agreement of the wave surface profiles as reproducing the plunging wave collapsing, running up and overtopping processes. The results of this study show that the WCSPH method provides a useful tool to simulate complicated wave transformation as propagates over coastal structures.

5. Acknowledgements

The authors would like to acknowledge Dr. C. Crespo, University of Vigo Spain for his invaluable guidance and advice.

6. References

1- Hsiao, sh.Ch. and Lin, T.Ch., (2010), Tsunami-like solitary waves impinging and overtopping an impermeable seawall: Experiment and RANS modeling, Coastal Engineering, 57, p.1– 18.

2-Shao, S., Ji, Ch., Graham, D.I., Reeve, D.E., James, Ph.W. and Chadwick, A.J., (2006), Simulation of wave overtopping by an incompressible SPH model, Coastal Engineering, Vol. 53, p. 723–735.

3- Tsai, Ch.P., Chen, H.B. and Lee, F.Ch., (2006),*Wave transformation over submerged permeable breakwater on porous bottom*, Ocean Engineering , Vol. 33, p.1623 – 1643.

4- Stansby, P.K., (2003), *Solitary wave run up and overtopping by a semi-implicit finite-volume shallow-water Boussinesq model*, Journal of Hydraulic Research, 41 (6), p. 639–647.

5- Li, T.Q., Troch, P. and Rouck J.D., (2004), *Wave overtopping over a sea dyke*, Journal of Computational Physics, 198, p. 686–726.

6- Shen, Y.M., Ng, C.O. and Zheng, Y.H., (2004), *Simulation of wave propagation over a submerged bar using the VOF method with a two-equation* $k-\varepsilon$ *turbulence modeling*, Ocean Engineering , Vol. 31, p. 87–95.

7- Kato, F., Inagaki, S. and Fukuhama, M., (2005), *Wave force on coastal dike due to tsunami. Porc. 25th ICCE*, Orlando, p. 5150 –5161.

8- Rambabu, A.C. and Mani, J.S., (2005), *Numerical prediction of performance of submerged breakwaters*, Ocean Engineering, Vol. 32, p. 1235–1246.

9- Christou, M., Swan, C. and Gudmestad, O.T., (2008), *The interaction of surface water waves with submerged breakwaters*, Coastal Engineering, Vol. 55, p. 945–958.

10- Jie, C.H., Changbo, J., Shixiong, H. and Wenwei, H., (2010), *Numerical study on the characteristics of flow field and wave propagation near submerged breakwater on slope*, ActaOceanol Sin, Vol. 29, No 1, p. 88-99.

11- Wiryanto, L.H., (2010), *Wave propagation passing over a submerged porous breakwater*, Journal of Engineering Mathematics , Vol. 70, p. 129-136.

12- Khayyer, A., Gotoh, H. and Shao, S.D., (2008), *Corrected Incompressible SPH method for accurate water-surface tracking in breaking waves*, Coastal Engineering, Vol. 55, p. 236–250.

13- Lo, E. and Shao, S., (2002), *Simulation of near-shore solitary waves mechanics by an incompressible SPH method*, Applied Ocean Research , Vol. 24, p. 275–286.

14- Gomez-Gesteira, M., Cerqueiro, D., Crespo, C. and Dalrymple, R.A., (2005), *Green water overtopping analyzed with a SPH model*, Ocean Engineering, Vol. 32, p. 223–238.

15- Dalrymple, R.A. and Rogers, B.D., (2006), *Numerical modeling of water waves with the SPH method*, Coastal Engineering, Vol. 53, p. 141–147.

16- Gotoh, H., Shao, S. and Memita, T., (2004), *SPH-LES model for numerical investigation of wave interaction with partially immersed breakwater*, Coastal Engineering Journal, Vol. 46, No. 1, p. 39–63.

17- Shao, S., (2005), *SPH simulation of solitary wave interaction with a curtain-type breakwater*, Journal of Hydraulic Research, Vol. 43, No. 4, p. 366-375.

18- Shao, S., (2006), *Incompressible SPH simulation of wave breaking and overtopping with turbulence modeling*, International Journal for Numerical Methods In Fluids, Vol. 50, 597–621.

19- Kim, N.H. and Ko, H.S., (2008), *Numerical Simulation on Solitary Wave Propagation and Run-up by SPH Method*, KSCE Journal of Civil Engineering, Vol. 12, No. 4, p. 221-226.

20- Kim, N.H., Kim, S.R. and Ko, H.S., (2010), *Numerical Simulation of wave transmission over a submerged breakwater in wave flume by using SPH method*, The 2010 KSCE Annual Conference Journal, p. 2289-2292, Incheon, Korea.

21- Liu, X., Xu, H., Shao, S. and Lin, P., (2013), *An improved incompressible SPH model for simulation of wave–structure interaction*, Computers & Fluids, Vol. 71, p. 113–123.

22- Ohyama, T., Kioka, W. and Tada, A., (1995), *Applicability of numerical models to nonlinear dispersive waves*, Coastal Engineering, Vol. 24, p. 297–313.

23- Monaghan, J.J., (1992), *Smoothed Particle Hydrodynamics*, Annual review of astronomy and astrophysics, Vol. 30, p. 543–574.

24- Monaghan, J.J., (1994), *Simulating free surface flows with SPH*, Journal Computational Physics, Vol. 110, p. 399–406.

25- Liu, G.R., (2003), *Mesh Free Methods: Moving Beyond the Finite Element Method*, CRC Press, 692 pp.

26- Liu, M.B. and Liu, G.R., (2010), *Smoothed Particle Hydrodynamics (SPH): an Overview and Recent Developments*, Archives of Computational Methods in Engineering, Vol. 17, Issue 1, p. 25-76.

27- Wendland, H. (1995), *Piecewiese polynomial, positive definite and compactly supported radial functions of minimal degree*, Advances in computational Mathematics, Vol. 4, p. 389– 396.

28- Monaghan, J.J., (1989), *On the problem of penetration in particle methods*, Journal of Computational Physics, Vol. 82, p. 1 – 15.

29- Colagrossi, A. and Landrini, M., (2003), *Numerical simulation of interfacial flows by Smoothed Particle Hydrodynamics*, Journal of Computational Physics, Vol. 191, p. 448–475.

30- Dilts, G.A., (1999), *Moving-Least Squares-Particle Hydrodynamics I. Consistency and stability*, International Journal for Numerical Methods in Engineering, Vol. 44, p. 1115–1155.

31- Panizzo, A., (2004), *Physical and Numerical Modeling of Sub-aerial Landslide Generated Waves*, PhD thesis, UniversitadegliStudi di L'Aquila.

32- Guizien, K. and Barthelem, E., (2002), *Accuracy of solitary wave generation by a piston wave maker*, Journal of hydrodynamic research, Vol. 40, No.3.

33- Yoshizawa A., (1991), *Eddy-viscosity-type subgrid-scale model with a variable Smagorinsky constant and its relationship with the one-equation model in large eddy simulation*, Physics of Fluids, A3(8), p. 2007–2009.

34- Blin, L., Hadjadj, A. and Vervisch, L., (2003), *Large Eddy Simulation of Turbulent Flows in Reversing Systems*, Journal of Turbulence, No. 4, 1–12.

35-Crespo, A.J.C., (2008), *Application of the Smoothed Particle Hydrodynamics model SPHysics to free-surface hydrodynamic*, PhD Thesis, Universidad de Vigo.

36- Dalrymple, R. A. and Knio, O., (2001), *SPH Modeling of Water Waves*, Proc. Coastal Dynamics (ACSE), Lund, Sweden, pp. 779–787.

37- Crespo, A.J.C., Gomez-Gesteira, M. and Dalrymple, R. A., (2007), *Boundary Conditions Generated by Dynamic Particles in SPH Methods*, Computers, Materials, Continua. 5 (3), 173–184.